Realisation of CdS/Mn_3O_4 nanocomposites for potential photocatalytic applications

Lei Xue[1], James Caleb Peters Rathnakumar Peters[2], Sathish Chander Dhanabalan[2], Jayasakthi Madhaiyan[2], Rajesh Kumar Manavalan[3], Joice Sophia Ponraj[2] ✉

[1]*Institute of Physics and Technology, Ural Federal University, Yekaterinburg 620002, Russia*
[2]*Centre for Advanced Materials, Integrated-Inter-Department of LiWET Communications, Aaivalayam – Dynamic Integrated Research Academy and Corporations (A-DIRAC), Coimbatore 641046, India*
[3]*Institute of Natural Science and Mathematics, Ural Federal University, Yekaterinburg 620002, Russia*
✉ *E-mail: joice.ponraj@aaivalayam.com*

Published in Micro & Nano Letters; Received on 16th December 2019; Revised on 4th May 2020; Accepted on 13th May 2020

The present work reports the realisation of high-quality crystalline CdS/Mn_3O_4 (CM) nanocomposites by a simple cost-effective chemical method in air atmosphere. The authors have performed theoretical calculations and experimental analysis in order to understand the synthesised nanocomposites. X-ray diffraction results showed that the CM nanocomposites were cubic and orthorhombic mixed structure which is in good agreement with the theoretical studies. Field emission scanning electron microscopy images of CM confirmed the formation of well distributed nanocomposites. The outcomes of DFT calculations provide results for the bandgap calculation of pure CdS, Mn_3O_4 and the CM nanocomposites. Photoluminescence studies with interesting visible light absorption demonstrated the great potentiality of the as-synthesised nanocomposites towards photocatalytic applications that could be a detailed research scope for the authors' future studies.

1. Introduction: Semiconductor nanoparticles have unique size dependent optical properties, which are significant in optoelectronics. Especially, control over both nanocrystalline morphology and the crystal size simultaneously is posing a new challenge to synthetic chemists and materials scientists as it plays a significant role in applications point of view. Manganese, as one of the transition metals, is complex but interesting because of its variable oxidation states leading to different oxides forms (MnO, MnO_2, Mn_2O_3, Mn_3O_4 and Mn_5O_8) exhibiting promise for a wide range of applications. Interestingly, Mn_3O_4 can be used for preparing soft magnetic materials such as manganese zinc ferrite [1]. Nanometre-sized Mn_3O_4 with remarkably increased surface area and greatly reduced size are expected to display better performance in the above-mentioned application [2]. Manganese oxide (Mn_3O_4) is a transition metal with a direct bandgap of 1.2 eV [3], which is a potential material for technological applications in catalysis, ion exchange, high density magnetic storage media, solar energy conversion etc. [4]. Cadmium sulphide (CdS) is a prospective candidate for photocatalysis among the visible light active semiconductors CeO_2, WO_3, Fe_2O_3, Cu_2O and Bi_2S_3 owing to its appropriate band edge structure that absorbs light with a wavelength shorter than 520 nm [5]. The photocatalytic performance of CdS could be limited by its low charge carrier separation efficiency and poor photochemical stability [6]. These limitations might be overcome by coupling of CdS with a semiconductor having a narrow or a wide energy gap.

Recently, CdS and Mn_3O_4 nanoparticles have received considerable attention because of their potential application in the conversion of solar energy into electrical energy in a variety of semiconductor devices [7]. This combination of composite forms one of the most sensitive semiconductors known today, especially for the conversion of visible and near infrared radiations, providing bandgap matching and better photoconductivity results [8]. Based on the literature survey, there was no report found in the synthesis of CdS/Mn_3O_4 (CM) nanocomposites. This drives our interest to realise the above-mentioned nanocomposites and to understand its structure and bandgap by means of theoretical calculations.

Herein, we report the synthesis of CM nanocomposites using cost-effective chemical method. The synthesised nanocomposites are characterised by various physical techniques such as X-ray diffractometry (XRD) and field emission scanning electron microscopy (FE-SEM) to understand the crystal structure, particle size and surface morphology. The band structure calculations for the CM nanocomposites are also performed by density functional theory (DFT). To the best of our knowledge, CM composite has not been previously reported in the literature and this study has great potentiality for further evaluation of this composite in photocatalytic applications.

2. Experimental

2.1. Materials: The chemical reagents used were analytical reagent grade without further purification. Cadmium nitrate $Cd(NO_3)_2$ and manganese (II) chloride tetra hydrate $MnCl_2{\cdot}4H_2O$ were attained from ALFA AESAR A Johnson Matthey Company, Ward Hill, US and sodium sulphide ($Na_2S{\cdot}xH_2O$) and NaOH was obtained from Nice Chemical Company, Kochi, India were used as precursors. The glasswares used in this experimental work were acid washed. Ultrapure water was used for dilution and sample preparation.

2.2. Synthesis and characterisation: CdS nanoparticles were prepared by a simple chemical method as described in our previous work [9]. Mn_3O_4 nanoparticles were also prepared by the same method. To synthesise Mn_3O_4 nanoparticles, 1.979 g of $MnCl_2{\cdot}4H_2O$ dissolved in 100 ml of de-ionised water and 0.8 g of NaOH was dissolved in 100 ml de-ionised water separately. NaOH solution was slowly added to $MnCl_2{\cdot}4H_2O$ solution drop-by-drop under continuous magnetic stirring. After 1 h, the brown precipitate (Mn_3O_4) was washed with de-ionised water or ethanol and then dried at 90°C. The obtained CdS and Mn_3O_4 nanoparticles were then mixed and ground in the mole ratio of 1:1, and calcinated at 120°C for 2 h to form the CM nanocomposites. Fig. 1 shows the theoretically calculated crystal structures of CdS, Mn_3O_4 and CM nanocomposites.

The crystal structure and the size of the nanocomposites were determined by X-ray diffraction studies performed by GEXRD system with CuKα radiation ($\lambda = 1.5406$ Å) at room temperature. The size and morphology were studied and understood from field emission scanning electron microscopy (FE-SEM, FEI Quanta 250 FEG). The photoluminescence (PL) spectra were recorded by

doi: 10.1049/mnl.2019.0783

FLUOROLOG Horiba Jobin Yvon spectrophotometer. DFT calculations were performed within the framework of the density-functional theory using the plane-wave pseudopotential approach in the Cambridge Sequential Total Energy Package (CASTEP) codes. We have used the generalised gradient approximation (GGA) of Perdew–Burke–Ernzerhof (PBE) scheme to describe the exchange-correlation potential. At the present calculations, energy cut-off of the plane-wave was set to be 450 eV and the special points sampling integration over the Brillouin zone (BZ) were performed using a k-mesh of dimension $2 \times 2 \times 2$ k-points mesh according to Monkhorst–Pack scheme, the tolerances for geometry optimisation were set as the difference in total energy within 1×10^{-6} eV/atom.

3. Results and discussion: Fig. 2 shows the XRD patterns of uncoated CdS [9], Mn_3O_4 and CM nanocomposite. Evidently, the diffraction peaks at 18.01° (1 0 1), 28.90° (1 1 2), 31.01° (2 0 0), 32.34° (1 0 3), 36.09° (2 1 1), 36.48° (2 0 2), 38.03° (0 0 4), 44.42° (2 2 0), 45.42° (2 1 3), 48.30° (3 0 1), 49.85° (2 0 4), 50.76° (1 0 5), 53.87° (3 1 2), 56.01° (3 0 3), 58.51° (3 2 1), 59.88° (2 2 4), 60.68° (2 1 5), 63.01° (1 1 6), 18.01° (1 0 1), 18.01° (1 0 1), 62.9° (1 0 3) and 68.0° (1 1 2) observed in Fig. 2 matched well with tetragonal structure (JCPDS file No. 89-4837) [10], confirming the successful synthesis of Mn_3O_4. In comparison with Mn_3O_4 nanoparticles, the crystal phase of CM nanocomposites had both cubic (CdS) and tetragonal (Mn_3O_4) peaks that were observed due to new layer deposited on the CdS surface. The theoretical structure calculations of CdS, Mn_3O_4 and CM are in good agreement with the experimental XRD results.

The surface morphology from FE-SEM micrographs of the synthesised Mn_3O_4 nanoparticles and CM nanocomposite with different magnifications (1 μm and 500 nm) is depicted in Fig. 3. It is clearly evident that the morphology of the synthesised nanocomposites is well defined crystallite grains with distinct grain boundaries. On a careful investigation, we are able to observe remarkable differences in the size difference between the pure Mn_3O_4 nanoparticles having particle size of about 30 nm and CM nanocomposites with particle size around 50 nm. CM nanocomposites are bigger in size and well dispersed.

Fig. 4 demonstrates the room temperature PL study of Mn_3O_4 and CM nanocomposites. PL spectra for CdS nanoparticles were elaborately explained in our previous paper [9]. The PL study revealed the optical properties of the materials in understanding their electronic transitions, intrinsic point defects like oxygen vacancies. After exciting, three emission peaks are observed at around 361, 388 and 405 nm. The UV emission peak at 361 and

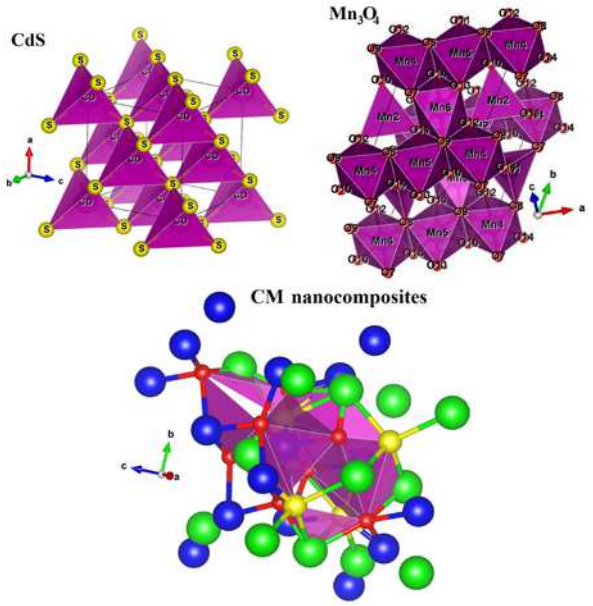

Fig. 1 *Crystal structures of CdS, Mn_3O_4 and CM nanocomposites from theoretical calculations*

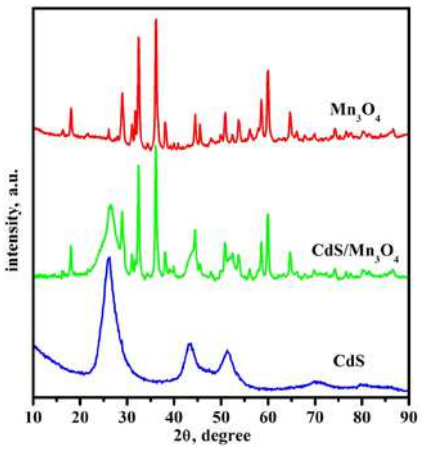

Fig. 2 *X-ray diffraction pattern of CdS, Mn_3O_4 and CM nanocomposites*

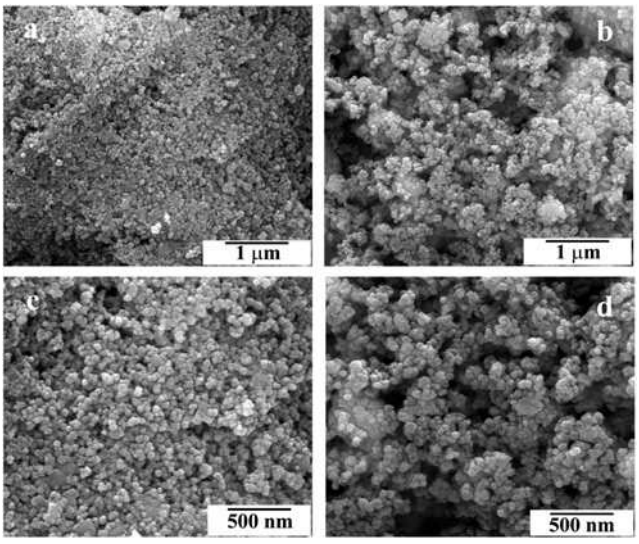

Fig. 3 *FE-SEM images with different magnifications (1 μm and 500 nm)*
a, *c* Mn_3O_4
b, *d* CM nanocomposites

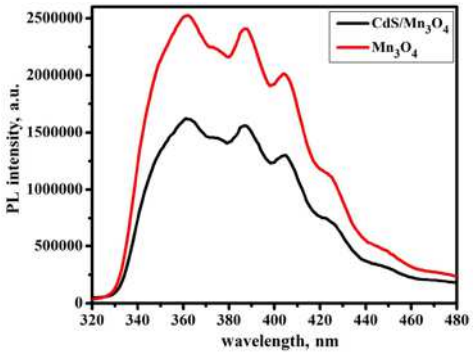

Fig. 4 *PL spectra for Mn_3O_4 and CM nanocomposites*

394 nm is attributed to the surface exciton recombination. The occurrence of UV band is mainly due to the electron–hole recombination and emission of the free exciton through an exciton–exciton collision of the well crystallised samples [11]. The photocatalytic activity can be explained based on PL intensity. In general, material with PL intensity will show less photocatalytic activity resulting from the recombination of electron–hole pair. Additionally, the observed low PL intensity for CM nanocomposites attributes its potential candidacy in having good photocatalytic properties. The recombination of electron–hole pair might be considerably less in CM composite materials with low PL intensity.

The energy band structure of CdS, Mn_3O_4 and CM nanocomposite has been calculated. From Figs. 5*a–c*, the value '0' corresponds to the Fermi energy. In Fig. 5*a*, it is clearly seen that the conduction band and valence band for CdS nanoparticles are, respectively, in the above and below Fermi level. The top of valence band and the bottom of conduction band are at the same point G corresponding to the direct bandgap semiconductor nature of CdS and the calculated bandgap is 1.564 eV in consistent with other result 1.05 eV [12], but smaller than the experimental value 2.42 eV [13].

From Fig. 5*b*, the top of valence band and the bottom of conduction band are not at the same point, which indicates that Mn_3O_4 is an indirect bandgap semiconductor with the calculated bandgap of 0.036 eV. In the case of CM nanocomposite (Fig. 5*c*), the top of valence band and the bottom of conduction band are not at the same point indicating that CM nanocomposite forms an indirect bandgap semiconductor and the calculated bandgap for CM nanocomposite is 0.031 eV. From the theoretical calculations, the bandgap is high for CdS nanoparticles and very low for CM nanocomposites.

Figs. 6*a–c* show that the energy levels in CdS, Mn_3O_4 spinel and CM nanocomposites could be divided into two parts: lower part called valence band and upper part of energy called conduction band. The spin polarisation of the material is defined as the difference between number of majority (spin-up) and minority (spin-down) electrons at the Fermi energy. The maximum spin polarisation is 100%. In these two bands, there is a symmetry between up and down spins, which allows us to get information related to the existence of magnetic properties of the materials. In this manner, Fig. 6*a* clearly portrays that there is a perfect symmetry between up and down spins establishing the absence of magnetic properties in CdS. In Fig. 6*b*, the symmetry spin channel is observed around −18 eV and there is a peak observed near Fermi

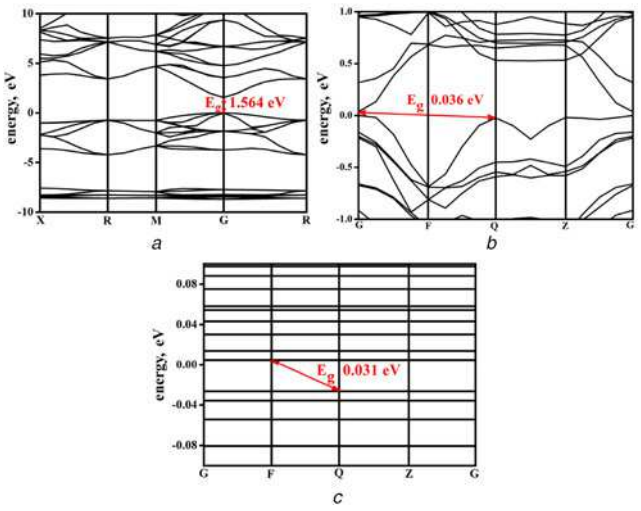

Fig. 5 *Energy band structure*
a CdS
b Mn_3O_4
c CM nanocomposite

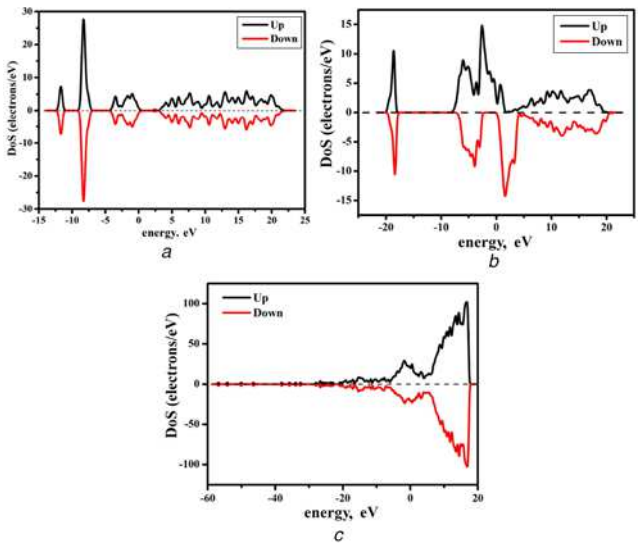

Fig. 6 *Spin DOS*
a CdS
b Mn_3O_4
c CM nanocomposite

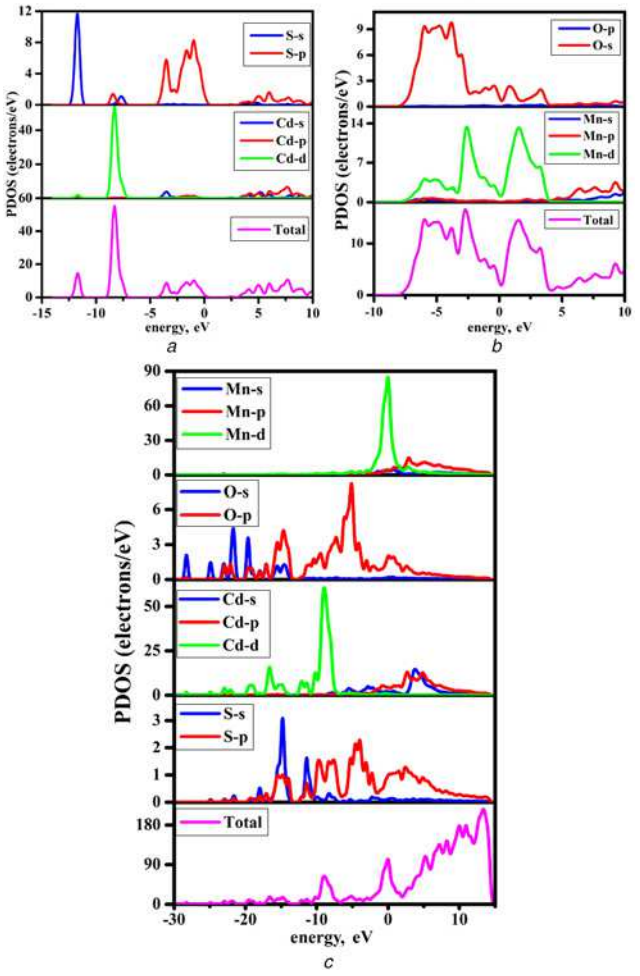

Fig. 7 *PDOS calculated*
a CdS
b Mn_3O_4
c CM nanocomposite

doi: 10.1049/mnl.2019.0783

level which is an evidence for the half-metallic ferromagnetic characteristics of Mn_3O_4 spinel as there is no coexistence of spin down and up is seen. Conversely, the minority-spin channel crosses the Fermi level in Fig. 6*c* shows the non-metallic characters of CM nanocomposites.

The total density of states (DOS) and partial DOS (PDOS) of CdS, Mn_3O_4 spinel and CM nanocomposites are given in Figs. 7*a*–*c*. It was understood from the previous literature [14] that DOS and PDOS can be used to understand the resulting properties in CdS emerging from the hybridisation of p-orbitals with d-orbitals of the transition metal. Interestingly, the DOS has the ability to explain the role of impurity atoms that can provide sufficient number of conduction holes near to the Fermi surface. The aforesaid variations might influence the electronic inter band transitions thereby causing a definite impact on the optical and dielectric properties [15].

The graphs of PDOS and DOS given in Fig. 7*a* present the distribution of DOS in the valence band evolved in three regions where peaks arise with wider and narrow distribution. The first peak is observable in the range between −4.4 and 0.1 eV due to Cd s-states and S p-states with least impact of Cd s-states. The second peak is quite narrow and lies between −9.1 and −7.1 eV involving the impact of Cd d-states and p-states of sulphur. Third DOS peak is located between −12.4 and −11.2 eV and shows contributions of high sulphur p-states and least Cd d-states. Correspondingly, Figs. 7*b* and *c* demonstrate the distribution of DOS in the valence band extended in three regions. In Fig. 7*b*, the first peak is in the range between 4.1 and 10 eV due to Mn p-states. The second peak is quite narrow and lies between −0.2 and 3.9 eV involving impact of Mn d-states and s-states of oxygen. Third DOS peak is located between −7.9 and 0.1 eV owing to the contributions of high oxygen s-states and Mn d-states. In Fig. 7*c*, the first peak is observable in the range between 14.8 and 1.9 eV attributed to Cd s, p-states and S p-states with least impact of Mn p-states. The second peak is quite narrow and is seen between −2.5 and 1.8 eV involving the impact of Mn d-states and p-states of sulphur. Third DOS peak is located between −9.8 and −7.1 eV with the contributions of Cd d-states and sulphur s, p-states.

4. Conclusion: High crystal quality CM nanocomposites were successfully synthesised. The synthesised nanocomposites exhibited strong visible light absorption and emission in the red region with large enhancement. The observed low PL intensity for CM nanocomposites attributes its potential candidacy in having good photocatalytic activity. This type of visible light absorption nanocomposites is the key aspect in the solar cell and photocatalytic applications. DFT calculations were performed on CdS, Mn_3O_4 spinel and CM nanocomposites, resulting in a consistent band structure with the characteristic band-splitting of the conduction band. The obtained CM nanocomposites could be further evaluated and studied for their potentiality in the field of hybrid photocatalyst in the future.

5. Acknowledgments: The author P. Joice Sophia kindly acknowledges DST-INSPIRE Faculty Scheme (DST/INSPIRE/04/2016/000292) and SERB-EMR (EMR/2017/004764) for the financial support and funding. One of the authors, M. Rajesh Kumar thanks the contract no. 40/is2.

6 References

[1] Al-Hada N.M., Kamari H.M., Shaari A.H., *ET AL.*: 'Fabrication and characterization of manganese-zinc ferrite nanoparticles produced utilizing heat treatment technique', *Results Phys.*, 2019, **12**, pp. 1821–1825

[2] Giri A., Goswami N., Sasmal C., *ET AL.*: 'Unprecedented catalytic activity of Mn_3O_4 nanoparticles: potential lead of a sustainable therapeutic agent for hyperbilirubinemia', *RSC Adv.*, 2014, **4**, p. 5075

[3] Javed Q., Feng-Ping W., Rafique M.Y., *ET AL.*: 'Canted antiferromagnetic and optical properties of nanostructures of Mn_2O_3 prepared by hydrothermal synthesis', *Chin. Phys. B*, 2012, **21**, p. 117311

[4] Ginsburg A., Keller D.A., Barad H.-N., *ET AL.*: 'One-step synthesis of crystalline Mn_2O_3 thin film by ultrasonic spray pyrolysis', *Thin Solid Films*, 2016, **615**, pp. 261–264

[5] Bao N., Shen L., Takata T., *ET AL.*: 'Self-templated synthesis of nanoporous CdS nanostructures for highly efficient photocatalytic hydrogen production under visible light', *Chem. Mater.*, 2008, **20**, pp. 110–117

[6] Kornarakis I., Lykakis I.N., Vordos N., *ET AL.*: 'Efficient visible-light photocatalytic activity by band alignment in mesoporous ternary polyoxometalate-Ag_2S-CdS semiconductors', *Nanoscale*, 2014, **6**, pp. 8694–8703

[7] Narayanan R., Deepa M., Friebel F., *ET AL.*: 'A CdS/Bi_2S_3 bilayer and a poly(3,4-ethylenedioxythiophene)/S^{2-} interface control quantum dot solar cell performance', *Electrochim. Acta*, 2013, **105**, pp. 599–611

[8] Jana A., Bhattacharya C., Datta J.: 'Enhanced photoelectrochemical activity of electro-synthesized CdS-Bi_2S_3 composite films grown with self-designed cross-linked structure', *Electrochim. Acta*, 2010, **55**, pp. 6553–6562

[9] Murugan R., Kumar M.R., Chander D.S., *ET AL.*: 'Facile and large scale aqueous synthesis of CdS nanoparticles at room temperature towards optoelectronic applications', *Mater. Res. Express*, 2018, **5**, p. 105003

[10] Rani B.J., Ravina M., Ravi G., *ET AL.*: 'Synthesis and characterization of hausmannite (Mn_3O_4) nanostructures', *Surf. Interfaces*, 2018, **11**, pp. 28–36

[11] Toufiq A.M., Wang F., Javed Q.U.A., *ET AL.*: 'Synthesis characterization and photoluminescent properties of 3D nanostructures self-assembled with Mn_3O_4 nanoparticles', *Mater. Express*, 2014, **4**, pp. 258–262

[12] Cheng Y.W., Tang F.L., Xue H.T., *ET AL.*: 'First-principles study on electronic properties and lattice structures of WZ-ZnO/CdS interface', *Mater. Sci. Semicond. Process.*, 2016, **45**, pp. 9–16

[13] Rajesh Kumar M., Murugadoss G.: 'Synthesis and study of optical and thermal properties of Mn doped CdS nanoparticles using polyvinylpyrrolidone', *J. Lumin.*, 2014, **146**, pp. 325–332

[14] Wrighton-Araneda K., Ruby-Figueroa R., Estay H., *ET AL.*: 'Interaction of H_2O with $(CuS)_n$, $(Cu_2S)_n$, and $(ZnS)_n$ small clusters ($n = 1$–4, 6): relation to the aggregation characteristics of metal sulfides at aqueous solutions', *J. Mol. Model.*, 2019, **25**, p. 291

[15] Khajuria S., Sanotra S., Khajuria H., *ET AL.*: 'Synthesis, structural and optical characterization of copper and rare earth doped CdS nanoparticles', *Acta Chim. Slov.*, 2016, **63**, pp. 104–112